Chapter 4

Lidar Mapping of Near-Surface Aerosol Fields

Tanja Dreischuh, Ivan Grigorov, Zahary Peshev, Atanaska Deleva, Georgi Kolarov and Dimitar Stoyanov

Additional information is available at the end of the chapter

http://dx.doi.org/10.5772/65274

Abstract

Near-surface atmospheric measurements over urban or industrial areas aimed at assisting the air-quality monitoring attain increasing societal significance due to the strong and direct impact of aerosol pollutions in the low troposphere on the human health. In this chapter, we present experimental results on lidar mapping of aerosol fields over the city of Sofia (Bulgaria), its suburbs and adjacent towns and villages, obtained during an extensive 7-month experimental campaign in 2015. The measurements are conducted by scanning observation zones in horizontal and vertical directions using lidar systems developed at the Institute of Electronics, Bulgarian Academy of Sciences. Based on the aerosol backscattering profiles retrieved at different azimuth or elevation angles, two-dimensional color-coded sector maps of the near-surface aerosol density are obtained, overlaid on the topological map of the Sofia region. The analysis of the lidar maps shows good correlation between the aerosol density distribution and the locations of important sources of aerosol pollutions in the zones of observation, such as city streets with intense traffic, industrial facilities, densely populated residential districts, etc. The results reported demonstrate that aerosol lidar mapping could be regarded as an effective approach for accurate and reliable determination of the density, spatial distribution, and temporal dynamics of close-to-ground aerosols, covering broad urban areas. Possibilities of incorporating synergistically lidar mapping technologies into municipal air-quality monitoring systems are also discussed.

Keywords: aerosol, lidar, scanning lidar, near-surface aerosol lidar mapping, air-quality monitoring

1. Introduction

The poor ecological state of the environment is a serious global problem which arose as a result of the rapid development of industry, agriculture, urbanization, and transport. Significant

factors affecting the state of the environment are both natural (hydrometeors, volcanic ash, desert dust, smoke aerosols, etc.) and anthropogenic (industrial, fuel combustion, fires, heating, etc.) atmospheric aerosols or particulate matter (PM) [1]. The aerosols are fine solid or liquid particles, determining largely the climate, temperature, and dynamic structure of the atmosphere, the functioning of ecosystems, the microphysical properties of clouds and various chemical and photochemical processes in air [2]. The concentration of aerosols in the atmosphere determines the air quality, and in turn affects the human health [[3] and references therein]. The fine and ultrafine aerosol particles are particularly harmful for human health, as they more easily penetrate and accumulate in the human body and lead to an increase in cardiovascular and respiratory diseases and even to lung cancer [4, 5]. Because of the above facts and considerations, atmospheric aerosols have been the subject of more intensive research in recent decades [6, 7]. Particularly, near-surface atmospheric measurements over densely populated or industrial areas, purposed to help monitor air quality, have attained increasing societal significance.

Laser radars (lidars) are recognized to be a reliable and powerful instrument for investigating atmospheric objects and air parameters [7–9]. As compared to other measurement approaches, the lidar technique exhibits advantages such as possibilities for performing fast, highly sensitive and accurate monitoring of vast atmospheric domains with high spatial and temporal resolution. Lidar systems are mainly used to assess the vertical structure of the aerosol layers and determine the optical and microphysical properties of the vertical profiles of the aerosols. Scanning ground-based and airborne lidars are applied to produce three-dimensional (3D) maps of earth's surface and man-made features [10], as well as for characterization of tropospheric wind profiles [11, 12] and temperature fields [13]. Along with the above applications, scanning elastic-scattering lidars are used to obtain maps of important atmospheric pollutants, particularly, of near-surface aerosol fields [14–17]. The aerosol lidar mapping represents a fast and effective approach to detect polluting aerosol loads over broad areas, as well as to characterize them in terms of local density, spatial distribution, and temporal dynamics [18–20].

In this chapter, we present experimental results on lidar mapping of near-surface atmospheric aerosol fields over the city of Sofia, its suburbs and surrounding villages, obtained during an extensive 7-month experimental campaign in 2015 [19]. It was carried out in the framework of a common project with Sofia Municipality aimed to help the local authorities to improve the regional air-quality monitoring. Possibilities are also discussed to incorporate lidar mapping technologies synergistically into municipal air-quality monitoring systems. Aerosol lidar maps are considered to become basic components of such monitoring systems. Their advantages result from the high efficiency of the laser light interaction with the atmospheric particles, thus, providing better visualization of atmospheric motions in comparison with other remote sensing techniques, such as the microwave or acoustic probing.

The analysis of the lidar mapping experiments performed was focused on the following issues:

i. Two-dimensional (2D) aerosol density distribution above the city areas.

ii. Temporal and spatial dynamics of the near-surface aerosol fields.

http://dx.doi.org/10.5772/65274

iii. Estimating effects of the city structure and terrain topography on the aerosol distribution obtained.

The chapter is organized as follows: In Section 2, we describe the experimental instrumentation, data processing/visualization approaches, and the area investigated. Then, in Section 3, series of experimental data on lidar aerosol mapping over the Sofia region are presented. Results are reported and analyzed of horizontal and vertical lidar scanning of the aerosol density distribution, as well as its temporal dynamics. Special attention is paid in Section 4 to the synergistic effects of mutual use of lidar aerosol mapping and in-situ measurement sites of the air pollution. The main results and conclusions are summarized in Section 5.

2. Experimental setup

2.1. Description of the area investigated

Sofia (the capital of Bulgaria) is located at about 550 m above sea level (a.s.l.), in a valley surrounded by hills and mountains, bordering Stara Planina to the northeast and Vitosha to the southwest. This topographic position, and the temperature inversion conditioned by it, is one of the factors determining the regional air quality. In the past years, the air pollution over the city of Sofia has become a serious ecological problem, provoked by the presence of different industrial facilities, a considerable decrease of green zones, as well as the accelerating growth of the population and the number of cars. The analysis of the PM amount and properties over Europe [21] showed that the aerosol concentrations have reached second-highest levels in eastern and southern Europe.

The measurement site (42.65N, 23.38E; 590 m a.s.l.) is located at the Institute of Electronics, Bulgarian Academy of Sciences, in the southeast part of Sofia. **Figure 1** shows a topographical map of Sofia area, overlaid by lidar sector scans in north-northwest (north-NW) (to the central parts of Sofia) and southwest (SW) (toward Vitosha Mountain) directions. In the former case, a horizontal lidar scanning (at a step of 1.7°) was performed in two close azimuth sectors of 8.5°(321–329.5° with respect to the north clockwise) and 17° (348–5°). In the latter case, the investigated sector was 50° (188–238°, at a step of 2°), whereas a low elevation angle (6–7°) was used to measure near-surface atmospheric aerosol fields because of the presence of high buildings in the angular sectors of measurements.

Under the conditions mentioned above, surface areas of about 100 km^2 were scanned and mapped over the central city zone, the north industrial zone and the south urban and suburb parts, including the north slopes of Vitosha Mountain. The results of the lidar aerosol mapping over these areas would allow one to detect and analyze the aerosols of different origin (natural, urban, industrial, etc.), as well as to contribute to the establishment of a modern city air-quality monitoring system.

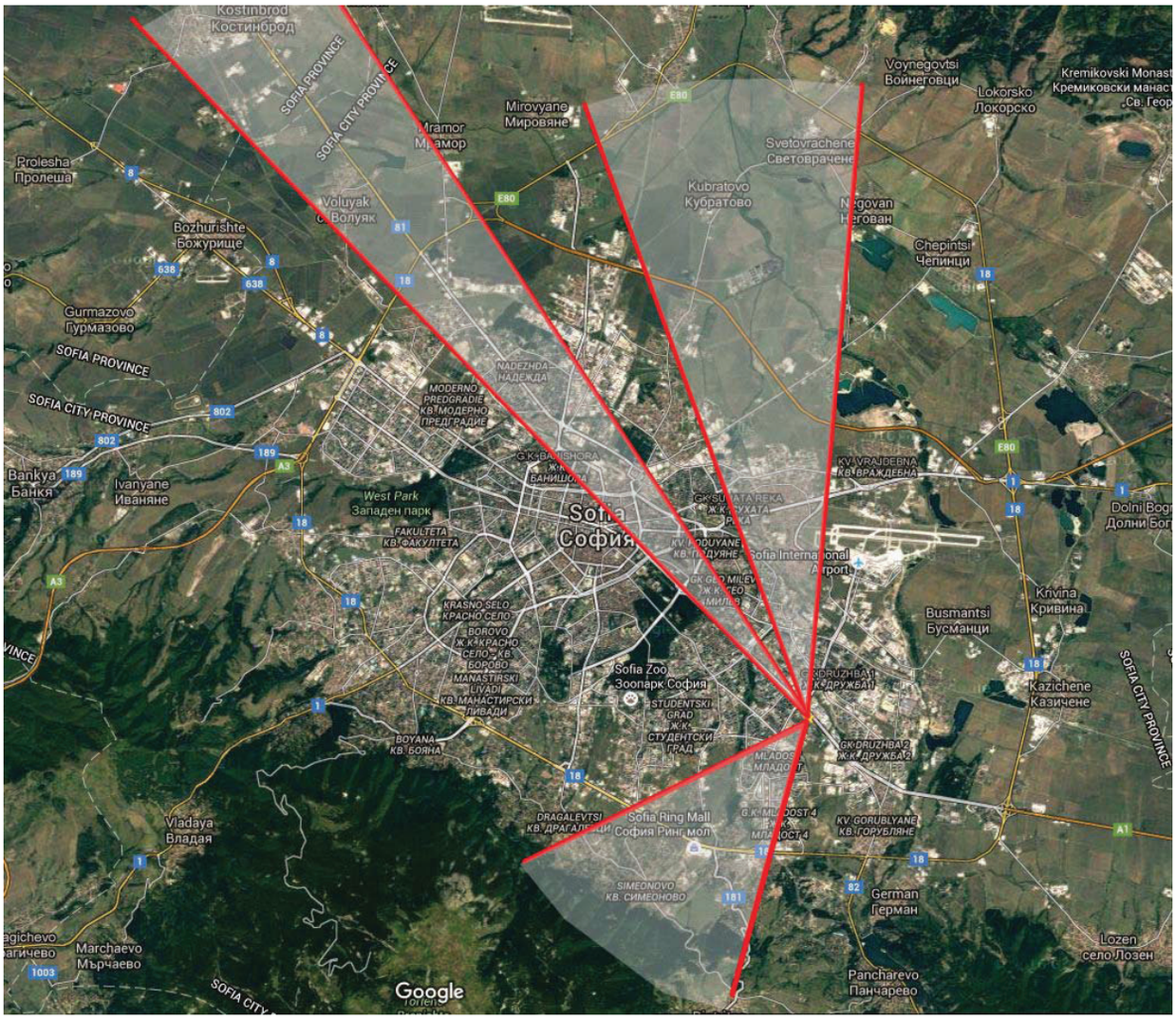

Figure 1. Topographical map of Sofia region with outlined azimuth sectors of lidar scanning.

2.2. Lidar systems

The measurements described in this chapter were conducted by scanning observation zones in horizontal and vertical directions over Sofia using lidar systems developed at the Laser Radars Laboratory of the Institute of Electronics, Bulgarian Academy of Sciences (LRL-IE). The LRL-IE working groups actively participate in the joint lidar research over the European continent in the framework of the European Aerosol Research Lidar Network, performing systematic lidar monitoring of atmospheric processes [18, 22], unusually high concentrations of aerosols in the troposphere [23], transport of mineral dust from Sahara desert [24], volcanic eruptions [25], and formation of smoke layers resulting from forest or industrial fires [26].

The lidar systems used in the experimental campaign considered are shown in **Figure 2**. The first one is based on a Cu-vapor laser emitting pulses with duration of 10 ns at a repetition rate of 5 kHz and wavelengths of 510.6 and 578.2 nm. Their mean powers are 1.2 and 0.8 W, respectively. The beam divergence is about 2 mrad. The laser beam is directed in parallel to

http://dx.doi.org/10.5772/65274

Figure 2. Photographs of the Cu-vapor (a) and Nd:YAG (b) laser-based lidars used in the aerosol lidar mapping experiments.

the axis of the receiving telescope, forming a lidar base of ~30 cm between the axes. A Cassegrain-type telescope with 20 cm aperture and 1 m focal length receives the backscattered laser emission from the atmosphere. Narrow-band interference filters are used to separate the lidar signals. Registration in a photon-counting mode is applied. The single electron pulses, produced by the photodetector (a photomultiplier), are accumulated by a photon-counting board in a computer. This board allows registration of the backscattered lidar signal with a spatial resolution of 15 or 30 m in 1024 samples and variable averaging time. In the present experiments, the lidar profiles of the laser emission backscattered in the atmosphere were registered with an accumulation time of 1 min. In addition, averaging was performed by summation of the data of 5–10 profiles; thus, the effective measurement time for each profile amounted to 5–10 min in a single azimuth direction.

The lidar used to perform lidar mapping experiments in the south-southwest direction is based on a solid-state frequency-doubled Nd:YAG laser (pulse energy of up to 600 mJ at 1064 nm, 80 mJ at 532 nm; fixed repetition rate of 2 Hz, FWHM pulse duration of 15 ns, beam divergence of 2 mrad), acting as a two-wavelength lidar transmitter. The optical part of the lidar receiver consists of a Cassegrain-type telescope (aperture 35 cm; focal distance 200 cm) and a three-channel spectrum analyzer based on narrow-band interference filters (1–3 nm FWHM). The receiver's electronic part comprises three compact photoelectronic modules, each including a photodetector, a 10 MHz 14-bit analog-to-digital converter (ADC), a high-voltage power supply, and controlling electronics. The signals backscattered in the atmosphere are digitized every 100 ns by the ADC, resulting in a 15 m range resolution. The system provides detection and storage of lidar returns from distances of up to 30 km. The lidar is mounted on a stable metal coaxial construction allowing reliable fixing and precise synchronized mutual motion of both the telescope and the output laser beam in horizontal and vertical direction with an angular resolution of about 1°.

2.3. Lidar data processing: deriving the atmospheric aerosol backscatter profiles

The lidar remote sensing is based on the interaction (absorption and scattering) of the laser light with molecules and aerosols in the atmosphere. The detected backscattered lidar signals contain information concerning the state and composition of the probed atmospheric domain. The so-called lidar equation describes the power of the received backscattered signal as a range-resolved function of the lidar parameters and the atmospheric optical properties (aerosol backscattering and extinction coefficients). For a single-scattering elastic lidar (measuring backscattered light at the same wavelength as the sensing laser wavelength λ) the power $P(r)$, detected at a time t after the instant of pulse emission, is written as [27]:

$$P(r) = P_0 \frac{c\tau}{2} A\varepsilon \frac{\gamma(r)}{r^2} [\beta_a(r) + \beta_m(r)] \exp\{-2\int_0^r [\alpha_a(\rho) + \alpha_m(\rho)] d\rho\}, \quad (1)$$

where P_0 is the average power of a single laser pulse, c is the speed of light, $r = ct/2$ is the distance along the laser beam path, τ is the pulse duration, A is the area of the receiver, ε is the overall system efficiency, γ(r) describes the overlap between the laser beam and the receiver field of view, and $\beta_a(r)$, $\beta_m(r)$ and $\alpha_a(r)$, $\alpha_m(r)$ are the backscattering and extinction coefficients for aerosols and molecules, respectively, at wavelength λ.

The determination of the aerosol extinction and backscattering coefficients (BSCs) on the basis of Eq. (1) requires the solution of a Bernoulli differential equation. A stable solution has been proposed by Klett [28] and Fernald [29], applying an inverse integration algorithm starting from the far end of the lidar sounding path. In the case of the backscattering coefficient (BSC), it has the following form:

$$\beta_a(r) = -\beta_m(r) + \frac{P(r) r^2 \exp\{-2[S_a(r) - S_m] \int_r^{r_{\text{ref}}} \beta_m(\rho) d\rho\}}{\frac{P(r_{\text{ref}}) r_{\text{ref}}^2}{\beta_a(r_{\text{ref}}) + \beta_m(r_{\text{ref}})} + 2\int_r^{r_{\text{ref}}} S_a(\rho) P(\rho) \rho^2 \exp\{-2[S_a(\rho) - S_m] \int_\rho^{r_{\text{ref}}} \beta_m(\rho') d\rho'\} d\rho} \quad (2)$$

where $S_a(r) = \alpha_a(r)/\beta_a(r)$ and $S_m = \alpha_m(r)/\beta_m(r) = 8\pi/3$ are the aerosol and the molecular extinction-to-backscatter lidar ratios, respectively. The reference range r_{ref} is chosen so that the aerosol backscatter coefficient at that point is either negligible compared to the molecular backscatter coefficient or is known from other sources. The vertical profiles of the $\beta_m(r)$ could be determined from the Standard Atmosphere Model [30] and from meteorological data. This algorithm is now widely applied in practice, assuming also that the aerosol lidar ratio S_a is invariant along the laser beam path. The exact value of this ratio is determined depending on the laser wavelength and also on *a priori* assumptions about the atmospheric conditions and the type of the aerosols observed.

In the case of lidar measurements in vertical or quasi-vertical directions, aerosol-free atmospheric domains are usually reached at certain altitudes (as a rule higher than 5–6 km) in the free troposphere, where the total backscatter coefficient $\beta(r) = \beta_a(r) + \beta_m(r) \approx \beta_m(r)$ is *a priori* known. In the case considered here of horizontal or quasi-horizontal lidar measurements, lidar

http://dx.doi.org/10.5772/65274

paths pass through close-to-surface atmospheric parts rich in aerosols, for which molecular reference values of $\beta(r)$ could not be used. In such cases, alternative and/or auxiliary approaches for retrieving the profiles of $\beta(r)$ have to be applied, in order to characterize the aerosol content in the observation areas. Such an approach is the so-called "slope method" [27], applicable to characterizing atmospheric domains with relatively homogeneous aerosol composition and concentration.

A typical feature of the atmosphere is its vertical stratification, expressed in the formation of a vertical succession of horizontally extended layers of different thickness. Inside these layers, the atmospheric air content and parameters remain practically constant over considerable horizontal distances. The longer the reachable lidar range of horizontal sounding, the higher the probability such homogeneous air volumes to be present along the lidar line of sight, providing favorable conditions for the method to be used. Thus, the slope method appears to be very suitable for determining aerosol characteristics in horizontal lidar measurements or such performed at low-elevation angles. The accuracy of this method increases with increasing the aerosol concentration, favoring its application to the lidar measurements conducted in the near-surface atmospheric layers where the highest aerosol concentrations are usually observed.

Applying the slope method to solving the lidar equation, one can obtain the following expressions for the aerosol extinction and backscattering coefficients:

$$\alpha_a(r) = \alpha_a = -0.5d\{\ln[P(r)r^2]\}/dr \tag{3}$$

and

$$\beta_a(r) = \beta_a = \alpha_a/S_a \tag{4}$$

Within the mentioned atmospheric parts of homogeneous aerosol parameters, S_a keeps empirically defined constant values depending on the aerosol types and densities. Both accuracy and reliability of the slope method increase proportionally to the lengths of the homogeneous parts present along the lidar beam path.

As an important advantage of the slope method, in comparison to other lidar approaches, determination of the aerosol extinction or backscattering is only or predominantly based on lidar measurement data, without the need of information or suppositions concerning relations between the analyzed quantities. In addition, the method makes use of simple mathematics, provides analytical solutions, and does not require numerical approaches and algorithms.

To implement the lidar mapping described here of the near-surface aerosol density distribution over Sofia region, a combination of the widely adopted and well-elaborated method of Klett-Fernald and the slope method was used. In this combination, the slope method is applied to determining the aerosol extinction and backscattering coefficients in appropriate parts of the lidar beam path by using the technology presented above (Eqs. (3) and (4)). Subsequently, the values of $\beta_a(r)$ obtained are used as reference (calibrating) ones in Eq. (2), in retrieving the whole range profiles of $\beta_a(r)$ by means of the Klett-Fernald approach. In this manner, the advantages of the two approaches are synergistically combined. As a result, the lidar range profiles of the aerosol extinction and backscatter coefficients are retrieved with relatively high

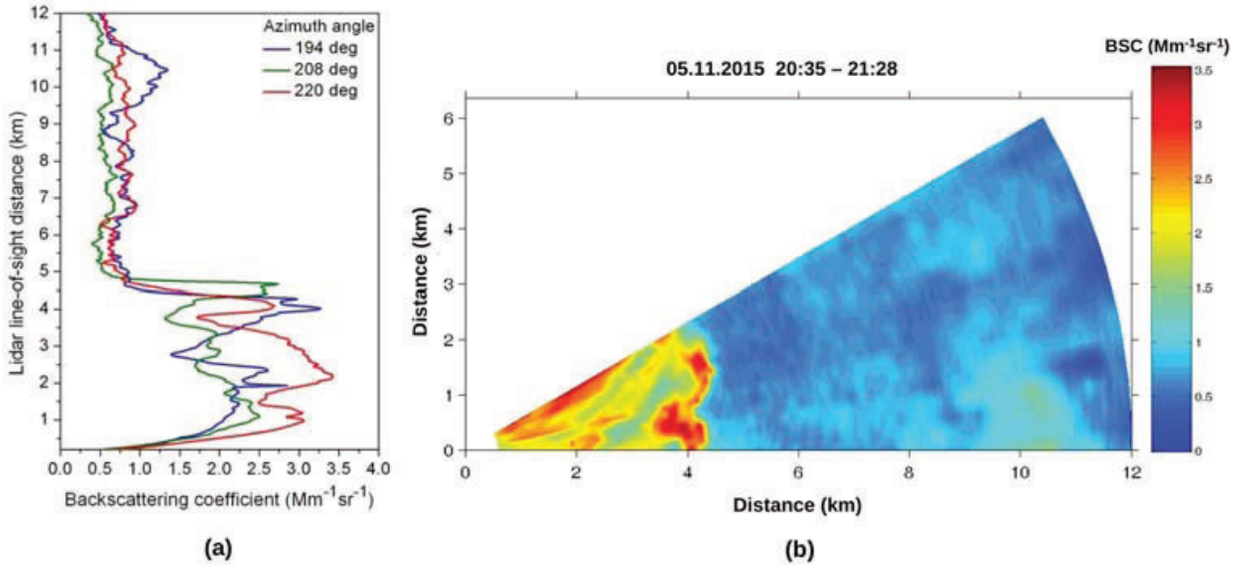

Figure 3. Range profiles of the aerosol backscattering coefficient at three different azimuth angles (a) and aerosol distribution lidar map based on a series of BCS profiles (b) as measured in the time interval 20:35–21:28 LT on 5 November 2015.

precision and reliability, which are accordingly transferred to the colormaps based on them of the near-surface aerosol density distribution.

2.4. Lidar mapping of aerosol fields

Generally, the aerosol field could be described as a distribution of the aerosol mass concentration M (μg/m^3) defined as the mass of PM per unit volume. From the lidar measurements, the extinction and backscattering coefficients of the aerosol particles are determined that are directly proportional to the aerosol mass concentration:

$$M = k\alpha_a = k\beta_a S_a. \tag{5}$$

The mass concentration could be retrieved from the lidar data combining different experimental and numerical approaches [31]. So, obtaining data about the distribution of the aerosol backscattering coefficient could be regarded as representative for the aerosol mass concentration distribution.

Figure 3 shows an example of the stages of formation of an aerosol lidar map using measurements performed on 5 November 2015, in the time interval 20:35–21:28 local time (LT). Aerosol backscattering profiles obtained at different azimuth angles along a fixed elevation angle are presented in **Figure 3(a)**. On the basis of a series of such profiles, 2D color-coded sector maps of the near-surface aerosol density could be created. In **Figure 3(b)**, an aerosol lidar map is displayed in Cartesian coordinates, based on the entire set of BSC profiles in the azimuth sector 190–220°, including the ones in **Figure 3(a)**. Finally, the sector maps so-obtained are superposed on the satellite maps of the corresponding city region.

http://dx.doi.org/10.5772/65274

3. Experimental results and discussion

Results of lidar measurements and mapping of the near-surface atmospheric aerosol fields over the city of Sofia, suburbs, and surrounding villages, obtained during the experimental campaign in 2015, are shown and discussed below. Lidar maps are presented from vertical and horizontal scanning of the areas investigated.

3.1. Mapping of aerosol fields by vertical scanning

In order to acquire detailed information about the vertical structure of the aerosol concentration, lidars perform vertical slice scans. The lidar data shown on **Figure 4** represent a two-dimensional color-coded sector map of the aerosol density distribution within the scanned volume of the atmosphere. The map is constructed using lidar profiles (averaged over five individual scans) obtained along a fixed azimuth in NW-direction at different elevation angles (0–10°), with an increment of 1°. The horizontal direction of the lidar scanning, covering

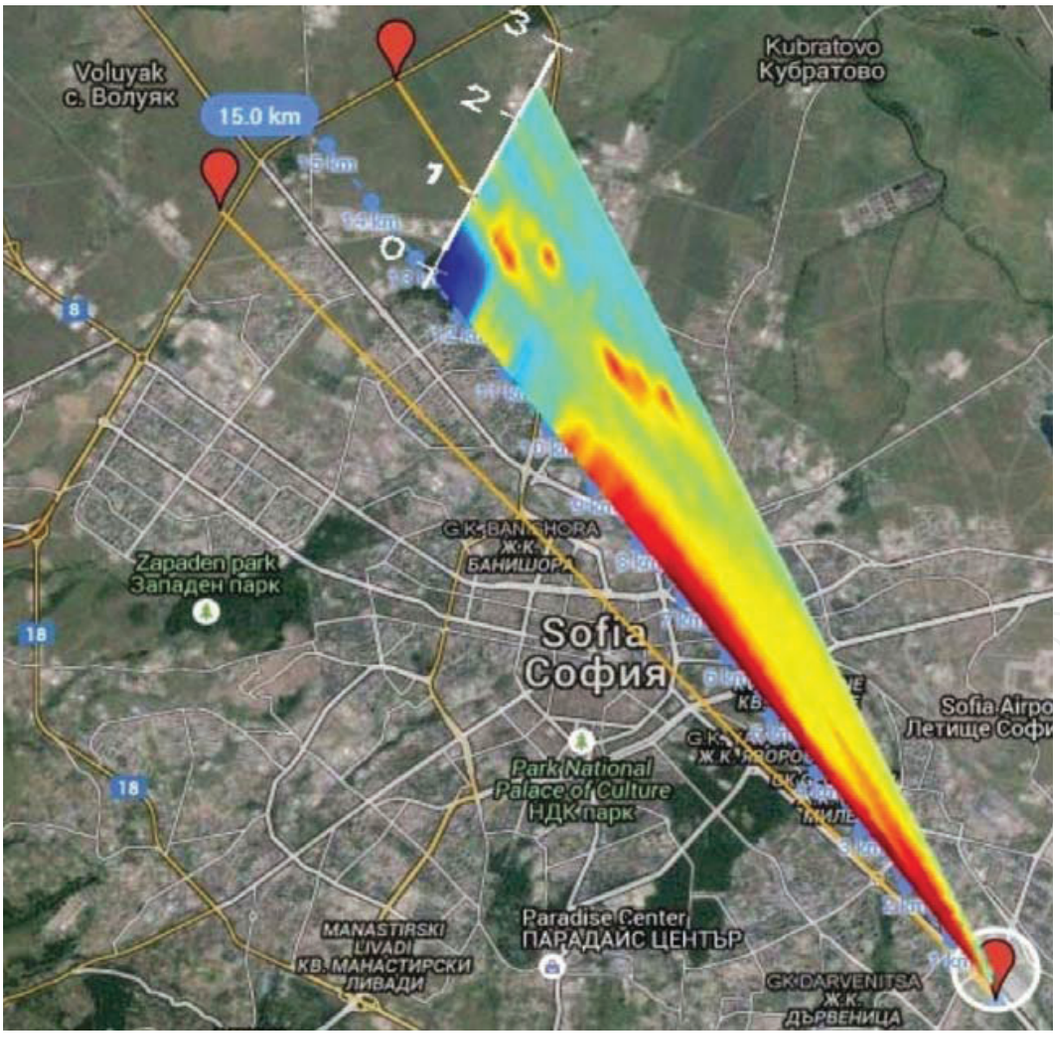

Figure 4. Color-coded sector map of the vertical aerosol density distribution obtained along a fixed azimuth in NW-direction (326° with respect to the north clockwise).

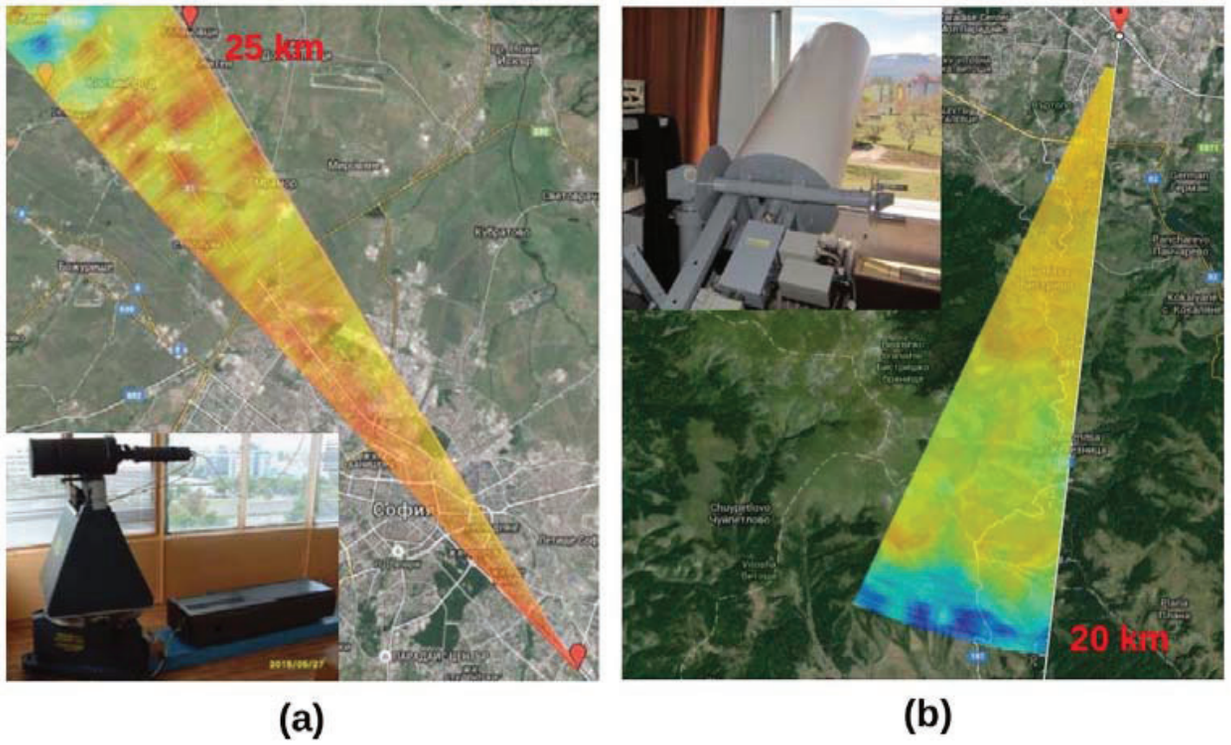

Figure 5. Colormaps of the near-surface aerosol density distribution demonstrating the maximum achievable operational distances in NW (a) and SW (b) directions, performed by the lidar systems shown in the insets.

distances of about 12 km was close to a thoroughfare with intense traffic. The vertical structure of the aerosol density of the atmosphere is clearly visible on the map. A well-pronounced vertical layer near ground surface was observed at a height in the range of 500–700 m, located above the city away from the lidar station until beyond the city center. At a height of ~1 km above ground, aerosol formations were observed with a density exceeding that of the ambient atmosphere, probably low clouds. Thus, this vertical map demonstrates the capability of such a type of lidar measurements to determine quickly and efficiently the location of the sources of anthropogenic PM emission in the atmosphere. On the other hand, it is clear that the horizontal scanning lidar measurements, made at a low altitude in the range of 500–700 m, provide sufficient information about the air pollution and near-ground surface aerosol fields.

3.2. Range limits of lidar measurements

Figure 5 illustrates the range limits of lidar measurements in NW (**Figure 5(a)**) and SW (**Figure 5(b)**) directions, performed by lidars with a Cu-vapor laser and a Nd:YAG laser, respectively. In the first case, the operational distance was from 900 m to 25–28 km in nighttime and decreased to about 10–15 km in daytime, due to intensive sky illumination. The maximum distance was limited by the high laser pulse repetition rate, because of an overlap of the laser pulse scattered from far away with the next pulse scattered from a close distance. In SW-direction to the Vitosha Mountain, the assessed maximum distance was longer than 20 km as determined by the surface topology in the observation area.

http://dx.doi.org/10.5772/65274

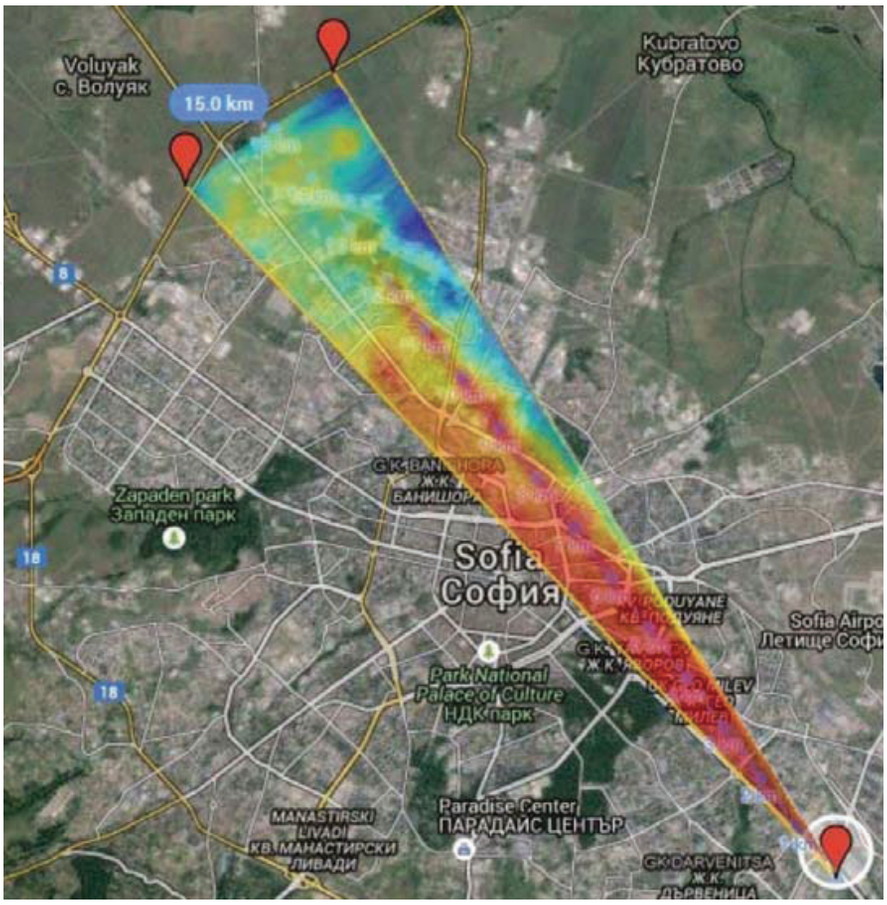

Figure 6. Colormap of the aerosol density distribution as measured on 27 July 2015 in the time interval 21:33–22:10 LT, at distances of up to 15 km.

3.3. Lidar mapping of aerosol fields over Sofia's central parts

Lidar monitoring and mapping of the near-surface aerosols in the atmosphere above the central parts of Sofia were performed by the lidar equipped with a Cu-vapor laser at the wavelength of 510.6 nm.

Figure 6 presents the results of lidar measurements carried out on 27 July 2015, at 21:33–22:10 LT, when relatively strong air pollution was observed. The distance covered by the lidar sounding was 15 km in an azimuth sector of 8.5°. A dust cloud was observed in the atmosphere near ground surface over most of the observation zone. Only the blue-colored areas, at 1.5–2 km away from the two large boulevards, showed a lower concentration of dust particles in the air. The specific movement of air masses, from SW-to-NE-direction, causes a mixing of dust pollutants into the larger part of the area over the city observed by the lidar. The values measured of the aerosol BSC are in the order of $0.5–8 \times 10^{-6}$ $m^{-1}sr^{-1}$.

Figure 7 presents results of lidar mapping in the two main sectors of scanning over the central parts of Sofia, performed in different time periods during the measurement campaign and exhibiting similar features of the aerosol distribution, in particular, the influence of populated areas on the aerosol density. The near-surface aerosol distribution, resulting from lidar

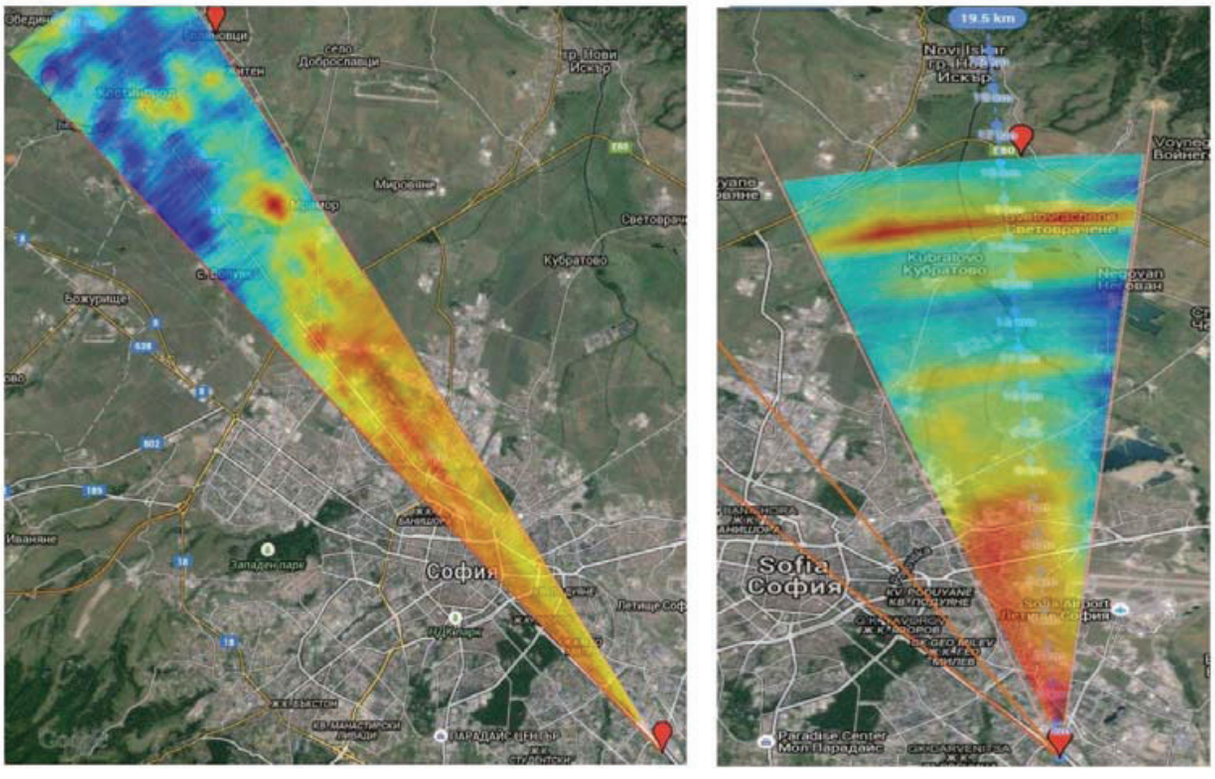

Figure 7. Color-coded maps of the near-surface aerosol density distribution as measured on 5 August 2015, at 22:10–22:50 LT (a) and on 7 October 2015 in the time interval 19:35–20:30 LT (b).

measurements performed on 5 August 2015, at 22:10–22:50 LT, is shown in **Figure 7(a)**, covering a distance of 25 km. Due to the heavy city traffic, relatively higher values of the aerosol BSC were observed close to the busy streets and over the entire central parts reaching the city ring road. At distances beyond the ring road, the aerosol pollution concentration dropped rapidly, except for some areas near two local villages. We, therefore, assumed that the aerosol fields observed by the lidar were of anthropogenic origin. The values measured of the aerosol BSC were in order of 0.3–4.3 × 10^{-6} $m^{-1}sr^{-1}$. **Figure 7(b)** presents a map of a lidar scanning conducted on 7 October 2015 within the NW sector, in the time interval 19:35–20:30 LT. The sounding comprised 11 successive scans in an angular sector of 17° by an angle step of 1.7°, covering a distance of 16 km. Well-defined areas of higher aerosol pollution were visible over the city areas, as well as over some residential districts in the far measurement zone. The values calculated of the atmospheric BSC were from 0.5 to 9.8 × 10^{-6} $m^{-1}sr^{-1}$.

In **Figure 8**, results are presented of lidar measurements in the two main sectors of scanning as in **Figure 7**, performed consecutively in the time intervals 19:22–19:48 and 19:54–20:54 LT on 4 November 2015. The first measurement (shown at the left angular sector of **Figure 8**) directed northwestward covered the central city zones including and being nearly parallel to one of the main city thoroughfare, reaching distances of up to 12 km. The second lidar sounding (shown at the right angular sector of **Figure 8**) was directed north-northwestward to distances of 13 km, covering densely populated residential districts in the part of the map near the lidar.

http://dx.doi.org/10.5772/65274

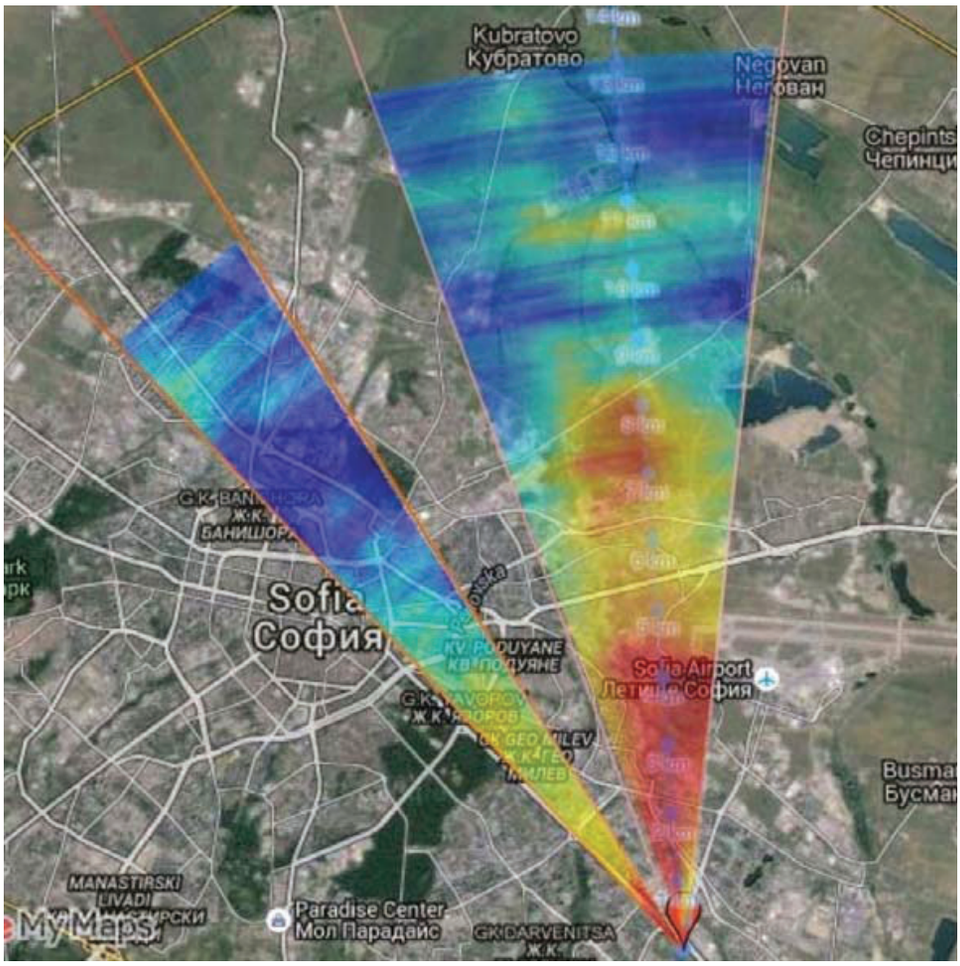

Figure 8. Color-coded maps of the near-surface aerosol density distribution as measured on 4 November 2015, in the time intervals 19:22–19:48 LT (left angular sector) and 19:54–20:54 LT (right angular sector).

Along this second direction, an area of high aerosol concentration was observed, which extended to a distance of 5 km with respect to the lidar. Another area of high concentration of the near-surface aerosols was observed at a distance of 7–8 km, at the end of the urban area. At greater distances, the aerosol air pollution observed was negligible, as shown by the green-blue colors in the figure. The BSC values calculated ranged from 0.5 to 6.2 × 10^{-6} $m^{-1}sr^{-1}$.

In order to demonstrate the capability of the lidar aerosol mapping technology applied to follow the temporal evolution of the near-surface aerosol density distribution, a series of successive lidar scans over the same areas were carried out. **Figure 9** presents four lidar maps resulting from measurements conducted on 18 November 2015, as averaged over 30 min intervals. The start times of each measurement are marked in the upper right corner of the corresponding figure panels. The measurements were implemented in the NW angular sector, reaching distances of up to 9.5 km. These maps illustrate the changes occurring in the near-surface aerosol fields measured over the city area in the observation zones. As can be seen, the areas located near the main city thoroughfare with the most intense traffic are colored in red-brown, indicating strong aerosol pollution, probably due to the car exhaust emissions. Inspecting the four pictures

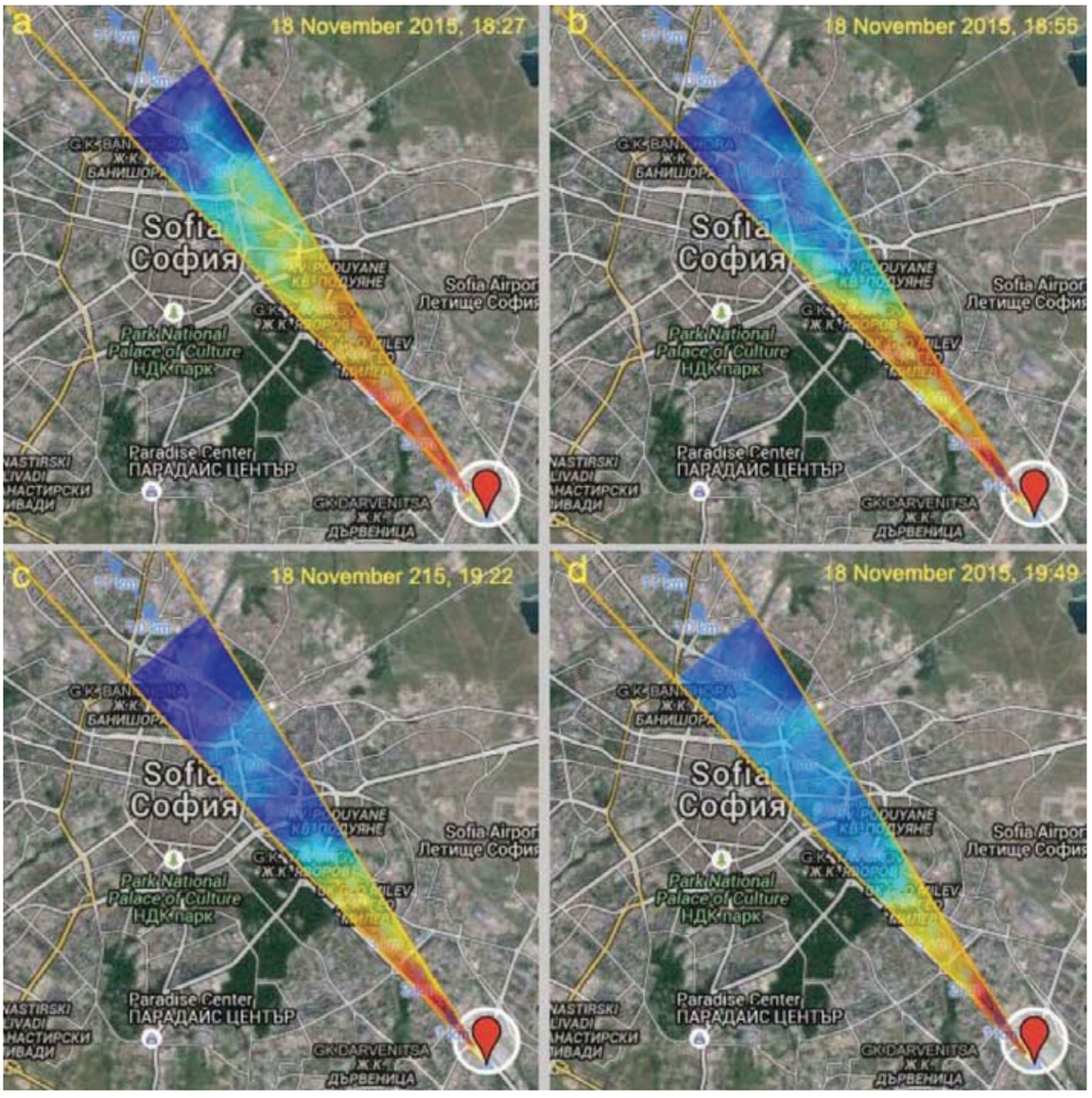

Figure 9. Color-coded maps of the aerosol density distribution as measured on 18 November 2015 in the time intervals 18:2718:52 LT (a), 18:55–19:20 LT (b), 19:22–19:47 LT (c), and 19:49–19:14 LT (d).

presented in their chronological order, one can perceive a progressive shrinking of the part of the maps polluted by aerosols. This peculiarity can be ascribed to the progressively diminishing traffic intensity in the evening hours, resulting in less car aerosol emissions.

3.4. Lidar mapping of aerosol fields toward Vitosha Mountain

Series of both daytime and nighttime lidar measurements of the near-surface aerosol density distribution were carried out in the period 3–9 November 2015. The meteorological conditions during the measurements were as follows: a relatively high temperature for the season (18–20° C); a weak wind; a stable temperature inversion within the atmospheric boundary layer (at altitudes 880–1200 m above ground level); atmospheric pressure: 970–920 hPa. These stable

http://dx.doi.org/10.5772/65274

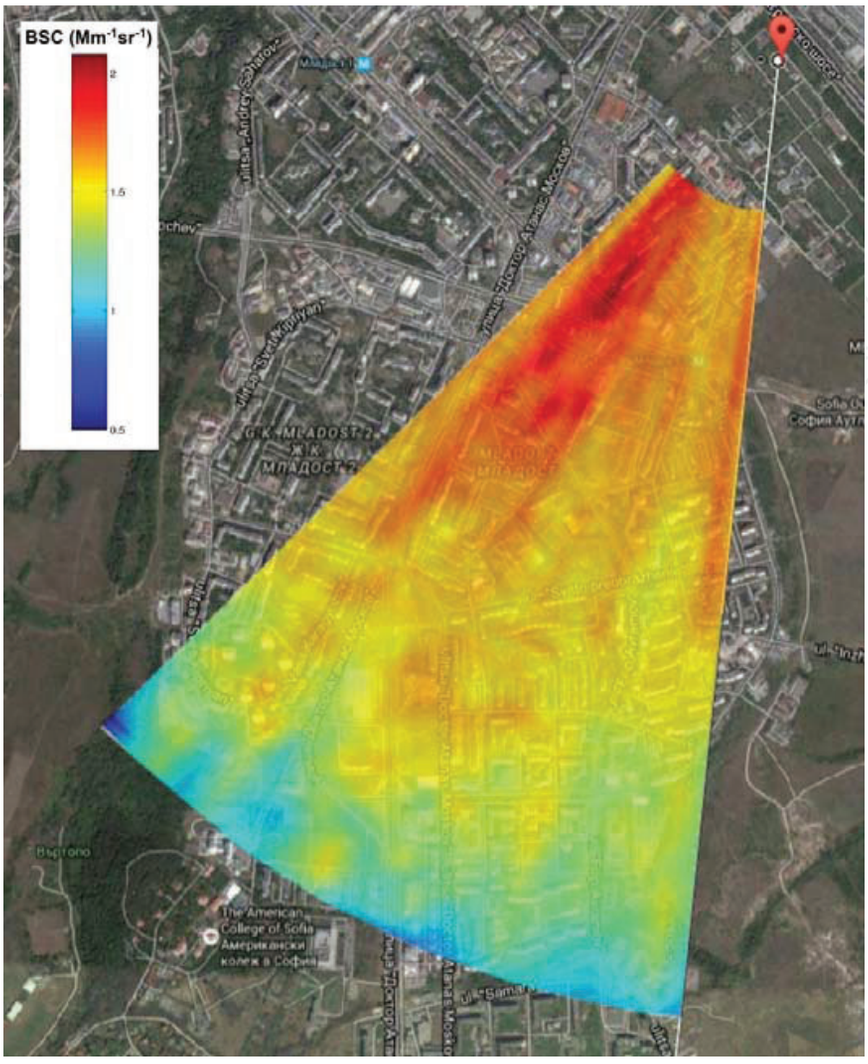

Figure 10. Colormap of the near-surface aerosol density distribution, as measured in the time interval 12:00–14:50 LT on 3 November 2015, in an azimuth range of 40° and distances of up to 3 km.

conditions, in combination with the absence of specific aerosol loadings (e.g. fire smoke, desert dust, etc.) in that period, resulted in aerosol distribution pictures generally similar to those obtained from the individual measurements conducted. Still, the lidar data exhibit particular patterns of the aerosol fields above the city, determined by various local horizontal and vertical air circulations in the close-to-the surface atmospheric layer.

Three separate lidar measurements were carried out on 3 November 2015—one in the first half of the day and two successive ones in the evening. During the daytime measurement, the lidar scanning was performed in south-southwest directions within a horizontal angle range of 40° to distances of up to 3 km. The results are shown in **Figure 10**. The correspondence between the aerosol BCS values and the lidar map colors is given by the color bar in the upper left corner. Inhomogeneous distribution of the aerosol concentration was registered, according to the spotted colormap pattern. In the left-hand upper part of the map, a dark-red colored area can be seen, extending to about 1 km and corresponding to the highest aerosol loading. This

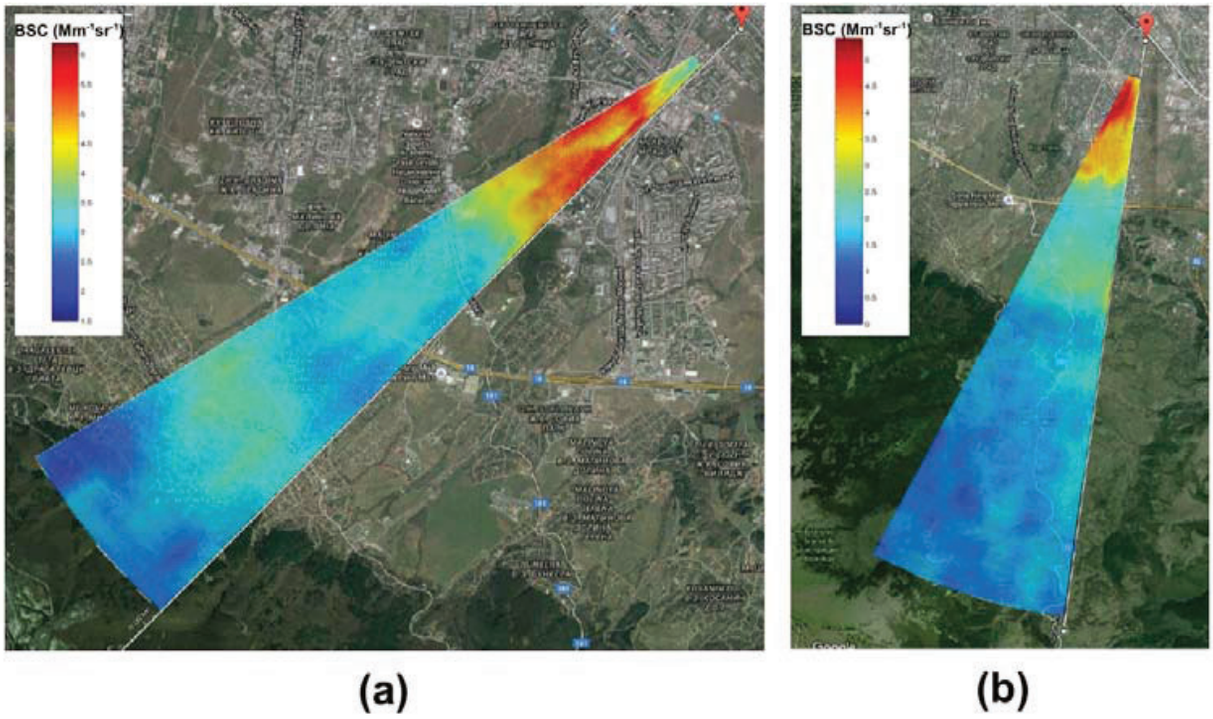

Figure 11. Colormap of the aerosol density distribution as measured on 3 November 2015 in the time interval 19:05–19:41 LT at distances of up to 8 km (a) and in the interval 19:56–20:40 LT at distances up to 12 km (b).

observation is reasonable, taking into account the fact that in this part of the city densely populated residential districts are located, with intense daytime street traffic.

In the evening of 3 November 2015, two successive lidar soundings were performed, the results of which are presented in **Figure 11**. Juxtaposing data of such successive measurements conducted in the same angular sector allows one to follow temporal variations of the aerosol fields over the areas investigated.

The first measurement was carried out by horizontal lidar scanning in an angular sector of 14°, reaching distances of up to 8 km (**Figure 11(a)**), whereas the second one, in a sector of 20° to a distance of 12 km (**Figure 11(b)**). The larger distances reached during the evening measurements are due to the much lower optical background than the daytime one. The comparison of the daytime (**Figure 10**) and nighttime (**Figure 11(a)**) lidar soundings showed that the relatively high concentration of aerosols measured at midday over the zone to 3 km near the lidar was preserved until the evening. At longer distances (beyond the ring road), approaching the Vitosha Mountain, the aerosol concentration decreased and remained relatively homogeneous, as indicated by the low-contrast light-bluish coloring of the corresponding map parts.

As an exception, an increased aerosol density could be observed over some remote parts of the scanned region in the distance range 4–6 km (colored in light green-yellow), where residential districts are located in the mountain skirts. This can be ascribed either to the presence of a light fog or to smoke emissions taking into account the started heating season.

http://dx.doi.org/10.5772/65274

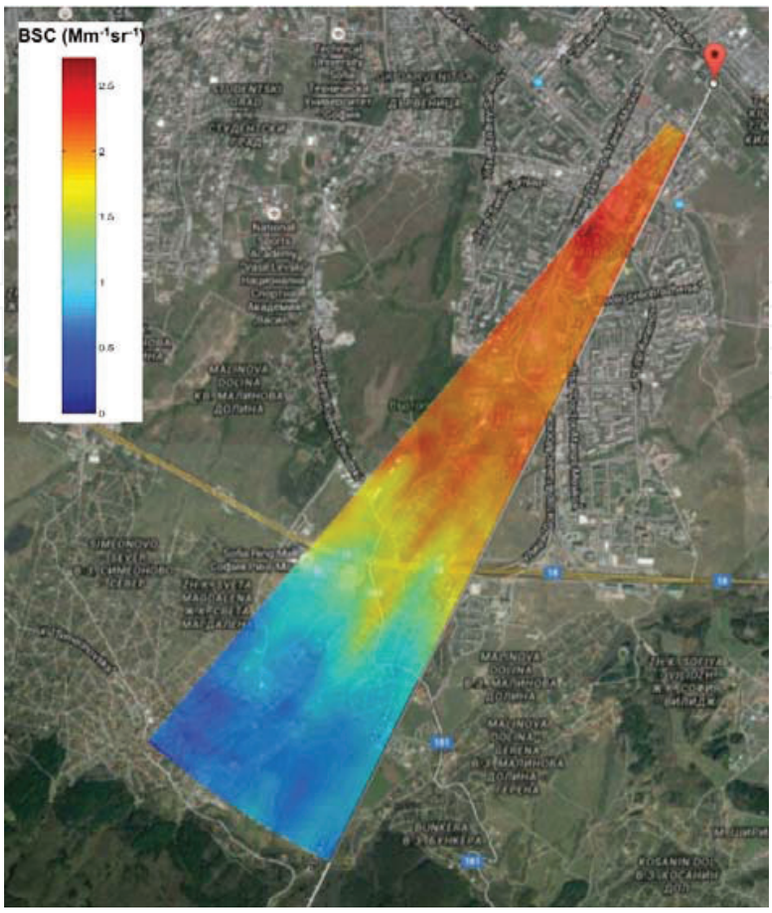

Figure 12. Colormap of the aerosol density distribution as measured on 5 November 2015 in the time interval 12:26–13:25 LT at distances of up to 7 km.

Four measurements were conducted on 5 November 2015 – one daytime over distances of up to 4 km and three successive nighttime ones over distances of up to 11 km. The daytime measurement was carried out in an angular sector of 14° and distances of up to 7 km. The highest aerosol loading was observed above the city zone about 4 km away from the lidar station, reaching the ring road, with a relatively homogeneous aerosol density distribution (**Figure 12**). These results are comparable to the ones presented above obtained during the daytime lidar measurements performed on 3 and 4 November 2015. This is reasonable because of the similar meteorological conditions and the absence of unusual aerosol pollutions.

All three nighttime lidar measurements took place in successive 1 h time intervals, over the same area in an angular sector of 30° and distances up to 12 km. The results are presented as colormaps in **Figure 13**. The comparison of the three panels shows the disappearance of the dynamic atmospheric processes, resulting in a considerable redistribution of the near-surface aerosol density. This can be clearly seen in the figure panels as expressed by the variable color pattern of the maps, most evident in the zones near the lidar extending to 4–5 km (colored mainly in red and yellow). In addition, the extension observed of the blue-colored remote part of the colormap sectors to the city zone in the course of the measurements could be ascribed to

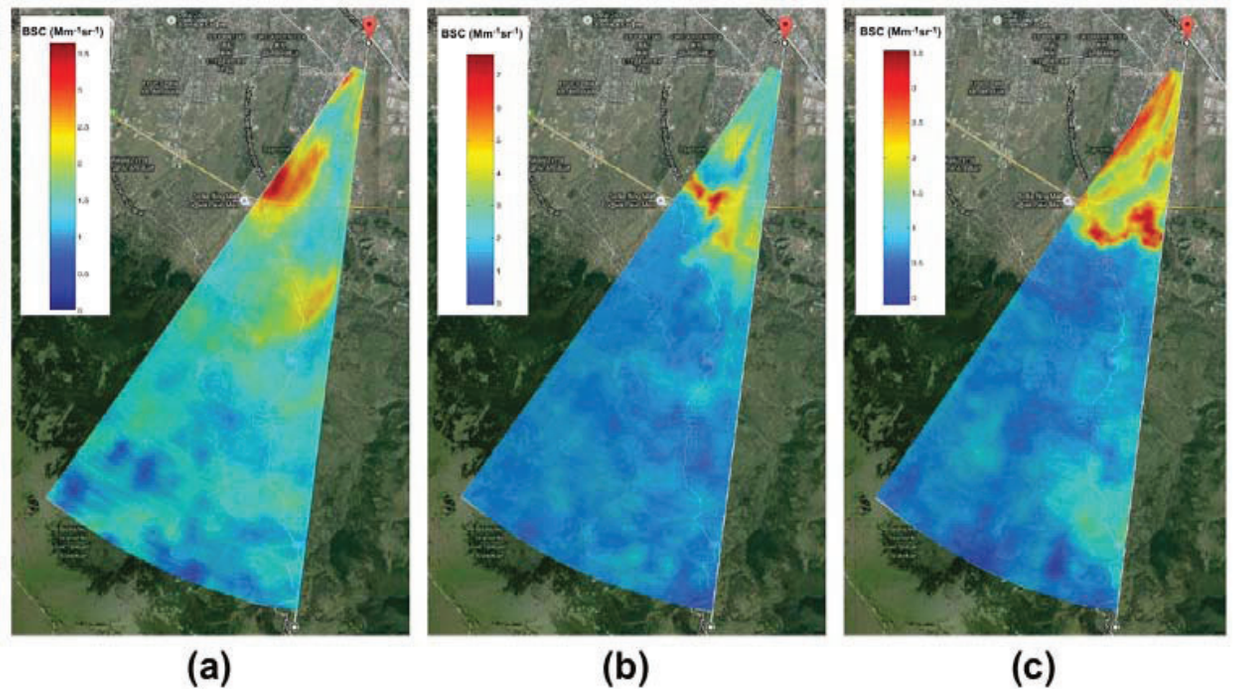

Figure 13. Colormap of the aerosol density distribution as measured on 5 November 2015 in the time intervals 18:37–19:33 LT (a), 19:36–20:29 LT (b) and 20:35–21:28 LT (c), at distances of up to 12 km.

movements of deficient in aerosols air masses from the mountain areas to the city, driven by the evening mountain breeze—characteristic of the Sofia region.

On 6 November 2015, three (two daytime and one nighttime) mapping lidar measurements were carried out within an angular sector of 26° over the same area. The two daytime measurements

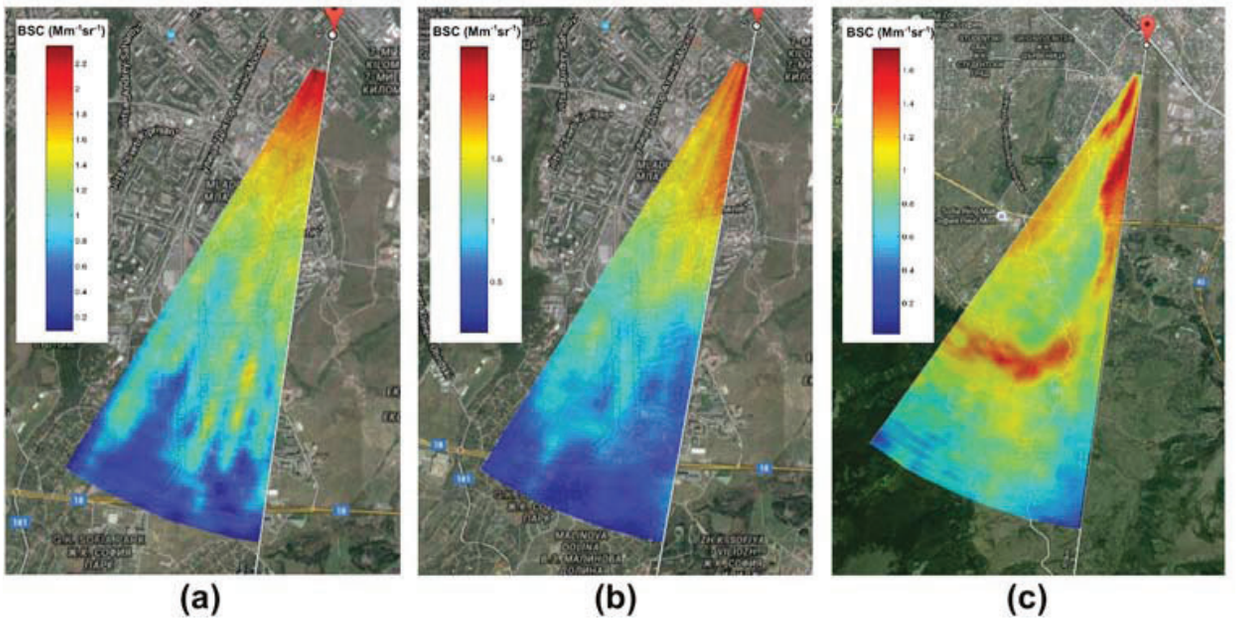

Figure 14. Colormap of the aerosol density distribution as measured on 6 November 2015 in the time intervals 10:24–11:39 LT (a), 11:48–11:53 LT (b) and 18:23–19:19 LT (c), at distances of up to 4 km (a, b) and 10 km (c).

http://dx.doi.org/10.5772/65274

covered distances of up to about 4 km, whereas the evening one, to nearly 10 km. The corresponding results are displayed as colormaps on the three panels of **Figure 14**. The analysis of the two daytime lidar maps (**Figure 14(a)** and **(b)**) revealed the highest aerosol densities in the 1 km zone near the lidar station (colored in red-yellow in the map). Examining the map color pattern, one can perceive gradations of coloring from dominating red in the near zone, through yellow-green in the middle part (forming stripe-like structures), to mainly blue approaching the mountain zone. This grading pattern might be explained as resulting from the action of air currents moving from the city to the mountain, capturing and transporting urban/anthropogenic aerosols to the mountain areas. The lidar data obtained during the nighttime mapping scans also support such an explanation. The colormap in this last case (**Figure 14(c)**) shows a particular aerosol distribution structure dominated by a folded aerosol plume (colored mainly in red and red-yellow) extending from the close-to-the lidar city zone, through the suburbs, up to the mountain skirts, and consisting of two differentiated but connected parts—a dense aerosol field over the urban zones and a similar one at the plane-mountain interface zone. This picture illustrates the complex nature and variability of the near-surface aerosol distribution and spreading, originating from different natural and anthropogenic sources and driven in a complex manner by the local air circulation system.

4. Synergy-based approach for incorporation of the lidar near-surface maps into modern air-quality monitoring systems

As shown in the previous sections, the aerosol lidar mapping technique is capable of providing a fast, accurate, and reliable range-time-resolved determination of optical parameters of the near-surface aerosols, such as the extinction and backscattering coefficients (directly proportional to the aerosol mass concentration), covering broad observation areas. In order to achieve complete quantitative aerosol characterization, determination of the aerosol mass concentration itself is also required. On the other hand, the existing set of in-situ air-pollution detectors present at some sites in the city is able to determine the aerosol mass concentration. However, this is possible to be done just for a limited number of detector location points. We consider that, by combining the two mentioned approaches, particularly by using in-situ obtained data to calibrate the aerosol lidar measurements, a synergistic effect could be achieved, allowing direct mapping of the aerosol mass concentration over the whole urban area. Below, we analyze and discuss the possibilities of achieving such a synergy in the characterization of near-surface aerosol pollutions.

As is well known, the typical existing air monitoring city systems contain the following basic structural components: (1) a network of a limited number of in-situ aerosol, gas, and biological sensors; (2) a network of meteorological sensors; (3) a modeling and data-processing system. The use of a low number of sensors by two networks over large urban areas imposes serious limitations on the information capabilities of the air-quality systems. The lidar maps can be considered as being a (virtual) aerosol sensor network of closely distributed very large number of single aerosol sensor cells of dimensions determined by the lidar maps' spatial resolution. Therefore, the lidar mapping of near-surface aerosol fields appears to be a promising

technology for improving the information quality of air-monitoring systems. The combination of the three sensor networks mentioned above incorporated in a joint air-quality monitoring system would provide a synergistic aerosol characterization.

Finally, we have to note that aerosol lidar maps could provide large amounts of additional information about the near-surface atmosphere. They contain data on the near-surface dynamics of air masses, driven by the surface winds but affected by the city structures. This is an important view of a better evaluation of the pollution transport over an urban area. Also, applying multiwavelength lidar mapping, one could contribute to the characterization of the aerosols' size parameters, as well as to identifying their types and origin.

5. Conclusions

Summarizing the results of lidar measurements presented here, one can draw the following conclusions:

1. Lidar mapping of near-surface aerosols, based on (quasi)horizontal and vertical lidar scanning using the two lidar systems of the LRL of IE-BAS, appears to be an effective approach to the accurate and reliable determination of the density, spatial distribution, and temporal dynamics of close-to-ground aerosols, covering broad urban areas in Sofia region.
2. The analysis of the two-dimensional aerosol lidar maps obtained, as superposed on the topological map of Sofia region, shows a good correlation between the aerosol density distribution and the locations of important sources of aerosol pollutions in the zones of observation, such as city streets with intense traffic, densely populated areas, etc.
3. Combining the near-surface aerosol lidar mapping technology with the existing set of in-situ air-pollution detectors and related numerical models and computing facilities, is shown to be a promising synergistic approach to the development of more efficient modern city air-quality monitoring systems.

Acknowledgments

The financial support of the Municipality of Sofia is gratefully acknowledged. The support for EARLINET in the ACTRIS Research Infrastructure Project by the European Union's Horizon 2020 research and innovation program under grant agreement no. 654169 and previously under grant agreement no. 262254 in the 7th Framework Programme (FP7/2007–2013) is also acknowledged.

Author details

Tanja Dreischuh*, Ivan Grigorov, Zahary Peshev, Atanaska Deleva, Georgi Kolarov and Dimitar Stoyanov

*Address all correspondence to: tanjad@ie.bas.bg

Institute of Electronics, Bulgarian Academy of Sciences, Sofia, Bulgaria

References

[1] European Environment Agency (EEA). The European Environment. State and Outlook 2010. Air Pollution. Luxembourg: Publication Office of the European Union; 2010. 46 p. DOI: 10.2800/57792

[2] Fuzzi S, et al. Particulate matter, air quality and climate: lessons learned and future needs. Atmos. Chem. Phys. 2015;**15**:8217–8299. DOI: 10.5194/acp-15-8217-2015

[3] World Health Organisation (WHO). Review of evidence on health aspects of air pollution —REVIHAAP Project. Technical Report. Copenhagen, Denmark: World Health Organisation, WHO Regional Office for Europe; 2013.

[4] Cesaroni G, et al. Long term exposure to ambient air pollution and incidence of acute coronary events: prospective cohort study and meta-analysis in 11 European cohorts from the ESCAPE Project. BMJ (Clinical research ed.). 2014;**348**:f7412. DOI: 10.1136/bmj.f7412

[5] Straif K, Cohen A, Samet J, editors. Air Pollution and Cancer. IARC Scientific Publication. Geneva, Switzerland: World Health Organisation; 2013. 161 p.

[6] Birmili W, et al. Atmospheric aerosol measurements in the German Ultrafine Aerosol Network (GUAN)—Part 3: Black Carbon mass and particle number concentrations 2009 to 2014. Gefahrstoffe Reinhaltung der Luft (Air Pollution Control). 2015;**75**:479–488.

[7] Sicard M, et al. EARLINET: potential operationality of a research network. Atmos. Meas. Tech. 2015;**8**:4587–4613. DOI: 10.5194/amt-8-4587-2015

[8] Kovalev V, Eichinger W. Elastic Lidar: Theory, Practice, and Analysis Methods. Hoboken, NJ, USA: Wiley-Interscience; 2004. 615 p. DOI: 10.1002/0471643173

[9] Pappalardo G, et al. EARLINET: towards an advanced sustainable European aerosol lidar network. Atmos. Meas. Tech. 2014;**7**:2389–2409. DOI: 10.5194/amt-7-2389-2014

[10] Shan J, Toth C, editors. Topographic Laser Ranging and Scanning: Principles and Processing. Boca Raton, FL, USA: Taylor and Francis; 2009. 590 p. DOI: 10.1080/01431160903112612

[11] Werner Ch. Doppler wind lidar. In: Weitkamp C, editor. Lidar. Range-Resolved Optical Remote Sensing of the Atmosphere. New York: Springer; 2005. pp. 325–354. DOI: 10.1007/b106786

[12] Pichugina Y, Banta R, Brewer W, Sandberg S, Hardesty R. Doppler Lidar-based wind-profile measurement system for offshore wind-energy and other marine boundary layer applications. J. Appl. Meteor. Climatol. 2012;**51**:327–349. DOI: 10.1175/JAMC-D-11-040.1

[13] Radlach M, Behrendt A, Wulfmeyer V. Scanning rotational Raman lidar at 355 nm for the measurement of tropospheric temperature fields. Atmos. Chem. Phys. 2008;**8**:159–169. DOI: 10.5194/acp-8-159-2008

[14] Behrendt A, Pal S, Wulfmeyer V, Valdebenito B. A-M, Lammel G. A novel approach for the characterization of transport and optical properties of aerosol particles near sources —Part I: measurement of particle backscatter coefficient maps with a scanning UV lidar. Atmos. Environ. 2011;**45**:2795–2802. DOI: 10.1016/j.atmosenv.2011.02.061

[15] Spuler S M, Mayor Sh D. Eye-safe aerosol lidar at 1.5 microns: progress towards a scanning lidar network. Proc. SPIE. 2007;**6681**:668102. DOI: 10.1117/12.739519

[16] Gao F, Bergant K, Filipčič A, Forte B, Hua D-X, Song X-Q, Stanič S, Veberič D, Zavrtanik M. Observations of the atmospheric boundary layer across the land–sea transition zone using a scanning Mie lidar. J. Quant. Spectrosc. Radiat. Trans. 2011;**112**:182–188. DOI: 10.1016/j.jqsrt.2010.04.001

[17] Xie C, Zhao M, Wang B, Zhong Z, Wang L, Liu D, Wang Y. Study of the scanning lidar on the atmospheric detection. J. Quant. Spectrosc. Radiat. Trans. 2015;**150**:114–120. DOI: 10.1016/j.jqsrt.2014.08.023

[18] Stoyanov D, Grigorov I, Kolarov G, Peshev Z, Dreischuh T. LIDAR atmospheric sensing by metal vapor and Nd:YAG lasers. In: Fadhali M, editor. Advanced Photonic Sciences. Rijeka, Croatia: Intech; 2012. pp. 345–374. DOI: 10.5772/29325

[19] Stoyanov D, Dreischuh T, Grigorov I, Kolarov G, Deleva A, Peshev Z, Nedkov I. Aerosol lidar mapping of large urban areas over Sofia Municipality. On the synergy with in-situ atmospheric sensors. Abstracts of the papers presented in the Fifth Scientific Meeting of the COST Action TD1105—New Sensing Technologies for Air-Pollution Control and Environmental Sustainability; 16–18 December 2015; Sofia, Bulgaria.

[20] He T-Y, Stanič S, Gao F, Bergant K, Veberič D, Song X-Q, Dolžan A. Tracking of urban aerosols using combined LIDAR-based remote sensing and ground-based measurements. Atmos. Meas. Tech. 2012;**5**:891–900. DOI: 10.5194/amt-5-891-2012

[21] Basart S, Pay M, Jorba O, Perez C, Jimenez-Guerrero P, Schulz M, Baldasano J. Aerosols in the CALIOPE air quality modelling system: evaluation and analysis of PM levels, optical depths and chemical composition over Europe. Atmos. Chem. Phys. 2012;**12**:3363–3392. DOI: 10.5194/acp-12-3363-2012

[22] Peshev Z, Dreischuh T, Toncheva E, Stoyanov D. Two-wavelength lidar characterization of atmospheric aerosol fields at low altitudes over heterogeneous terrain. J. Appl. Remote Sens. 2012;**6**:063581. DOI: 10.1117/1.JRS.6.063581

[23] Deleva A, Grigorov I. Lower troposphere observation over urban area with lidar at 1064 nm. IJNO. 2011;**2011**:1–8. DOI: 10.1155/2011/769264

[24] Peshev Z, Evgenieva Ts, Dreischuh T, Stoyanov D. Two-wavelength lidar characterization of optical, dynamical, and microphysical properties of Saharan dust layers over Sofia, Bulgaria. Proc. SPIE. 2015;**9447**:94470R. DOI: 10.1117/12.2175654

[25] Grigorov I, Stoyanov D, Kolarov G. Lidar observation of volcanic dust layers over Sofia. Proc. SPIE. 2011;**7747**:77470R. DOI: 10.1117/12.882795

[26] Grigorov I, Deleva A, Stoyanov D, Kolev N, Kolarov G. LIDAR detection of forest fire smoke above Sofia. Proc. SPIE. **7747**:77470U. DOI: 10.1117/12.2178791

[27] Measures R. Laser Remote Sensing: Fundamentals and Applications. New York: Wiley-Interscience; 1984; p. 510.

[28] Klett, J. Stable analytical inversion solution for processing lidar returns. Appl. Opt. 1981;**20**:211–220. DOI: 10.1364/AO.20.000211

[29] Fernald G. Analysis of atmospheric LiDAR observations: some comments. Appl. Opt. 1984;**23**:652–653. DOI: 10.1364/AO.23.000652

[30] United States Committee on Extension to the Standard Atmosphere (COESA). U.S. Standard Atmosphere 1976. U.S. Government Printing Office, Washington, D.C. 1976. 241 p.

[31] Ansmann A, Seifert P, Tesche M, Wandinger U. Profiling of fine and coarse particle mass: case studies of Saharan dust and Eyjafjallajökull/Grimsvötn volcanic plumes. Atmos. Chem. Phys. 2012;**12**:9399–9415. DOI: 10.5194/acp-12-9399-2012

IntechOpen